

# Draft – Effect of Atmospheric Heatwaves on Reflectance and Pigment Composition of Intertidal *Nanozostera noltei* – Draft

Simon Oiry<sup>a,\*</sup>, Bede Ffinian Rowe Davies<sup>a</sup>, Philippe Rosa<sup>a</sup>, Augustin Debly<sup>a</sup>, Anne-Laure Barillé<sup>b</sup>, Nicolas Harrin<sup>b</sup>, Pierre Gernez<sup>a</sup>, Laurent Barillé<sup>a</sup>

<sup>a</sup>*Institut des Substances et Organismes de la Mer, ISOMer, Nantes Université, UR 2160, F-44000 Nantes, France,*

<sup>b</sup>*Bio-littoral, Immeuble Le Nevada, 2 Rue du Château de l'Eraudière, 44300 Nantes, France,*

---

## Abstract

To be written

**Keywords:** Remote Sensing, Pigment Composition, Seagrass, Coastal Ecosystems, Heatwaves

---

## 1. Introduction

Intertidal seagrasses play a crucial role in the ecosystem by providing habitats and feeding grounds for various marine species, supporting rich marine biodiversity, and contributing significantly to primary production and carbon sequestration [1, 2]. These seagrasses are essential in maintaining the health of coastal ecosystems by stabilizing sediments, filtering water, and serving as indicators of environmental changes due to their sensitivity to water quality variations [3]. The interactions between seagrass meadows and their associated herbivores further enhance the delivery of ecosystem services, including coastal protection and fisheries support [4, 5, 6]. Understanding and preserving these ecosystems are vital for maintaining the biodiversity and productivity of coastal regions [7, 8].

Despite their crucial role in marine ecosystems, intertidal seagrasses face numerous threats that compromise their health and functionality. Coastal development and human activities are primary threats. These activities not only reduce the available habitat for seagrasses but also increase water turbidity, which limits light penetration and hampers photosynthesis [9]. Seagrasses are also

---

\*Corresponding author

Email address: [oiry\\_simon@gmail.com](mailto:oiry_simon@gmail.com) (Simon Oiry)

threatened by nutrient enrichment from agricultural and urban runoff, which can lead to eutrophication. This condition promotes the overgrowth of algal blooms that compete with seagrasses for light and nutrients, further stressing these important plants [10] (Oiry et al. 2024). Pollution from industrial and agricultural fields sources introduces harmful chemicals and heavy metals into coastal waters, posing toxic risks to seagrass health. These pollutants can affect the physiological processes of seagrasses, reducing their growth and survival rates [11]. Additionally, invasive species can out compete native seagrasses for resources, altering community structure and function [12].

Heatwaves, exacerbated by climate change, pose a growing threat to seagrasses. Marine Heatwaves (MHW), defined by [13] as prolonged discrete anomalously warm water events, and Atmospheric Heatwaves (AHW), defined by [14] as periods of at least three consecutive days with temperatures exceeding the 90th percentile, cause severe physiological stress on seagrasses [15, 16]. At the interface between the land and oceans, intertidal seagrasses are exposed to both MHW and AHW. Heatwaves have profound impacts on seagrasses, with their effects varying based on species and geographic location. For instance, the seagrass *Zostera marina* exhibits high susceptibility to elevated sea surface temperatures during winter and spring, leading to advanced flowering, high mortality rates, and reduced biomass [15]. Similarly, *Cymodocea nodosa* shows increased photosynthetic activity during heatwaves but suffers negative effects on photosynthetic performance and leaf biomass during recovery [16]. Additionally, different populations of *Zostera marina* along the European thermal gradient exhibit varied photophysiological responses during the recovery phase of heatwaves, indicating differential adaptation capabilities among populations [17]. These events intensify other stressors, such as overgrazing and seed burial, compromising sexual recruitment [18].

Remote sensing is increasingly being used to monitor marine ecosystems, including seagrass meadows. Spectral indices such as the Normalized Difference Vegetation Index (NDVI) and the Soil-Adjusted Vegetation Index (SAVI) are effective for quantifying vegetation health over time [19, 20, 21, 22]. By analyzing specific spectral patterns, remote sensing can track changes in seagrass meadows with high temporal and spatial resolution. Europe promotes these techniques through frameworks like the Water Framework Directive and the Marine Strategy Framework Directive, which advocate for habitat mapping using remote sensing technologies to cover large areas and detect long-term trends [23].

This study aims to experimentally test the hypothesis that warm events, such as atmospheric heatwaves, alter the pigment composition and reflectance of the intertidal seagrass *Nanozostera noltei*. By linking these changes with satellite remote sensing data, the study seeks to provide insights into how heatwaves affect seagrass meadows and to assess the potential of remote sensing in monitoring these impacts

## 2. Material & Methods

### 2.1. Observation of seagrass leaves darkening.

#### 2.1.1. Field Observation

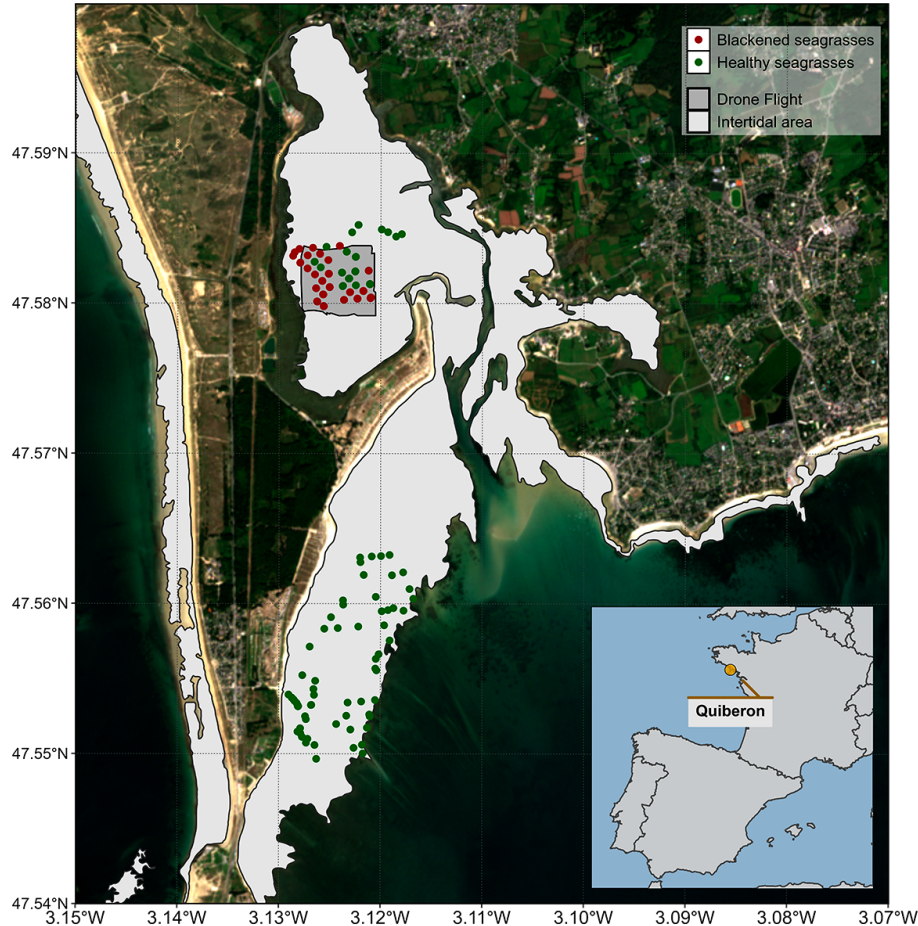


Figure 1: Location of the fieldtrip campaign that occurred in the 10th of September 2021. The light grey polygons indicates the intertidal zone (Zone between High tide and low tide, that is totally emerged at low tide) and the dark grey polygon indicate the extent of the drone flight. Green dots indicate location of quadrat picture over green seagrasses while red dots indicate location of quadrat took over darkened seagrasses.

A fieldtrip, aiming to map a seagrass meadow near Quiberon (France : 46°57'32.0"N, 2°10'37.0"W), occurred in the 10th of September 2021 (Figure 1). During this fieldtrip, darkening of seagrasses have been observed, resulting in the darkening of seagrass leaves over large area of the meadow (Figure 2 C & D). During this field trip, drone flights were conducted over two areas of the seagrass meadow using a DJI Matrice 200 equipped with a Sequoia

Multispectral camera. The Sequoia captures four spectral bands: Green ( $550 \pm 40$  nm), Red ( $660 \pm 40$  nm), RedEdge ( $735 \pm 10$  nm), and Near Infrared ( $790 \pm 40$  nm). A total of 122 Ground Control Points (GCPs) were collected in the form of georeferenced quadrat images across the meadow. These images allow for visual assessment of vegetation type, density, and health status. The images were then divided into two categories: green seagrasses and darkened seagrasses, based on a visual estimation of the leaf condition (Figure 1).

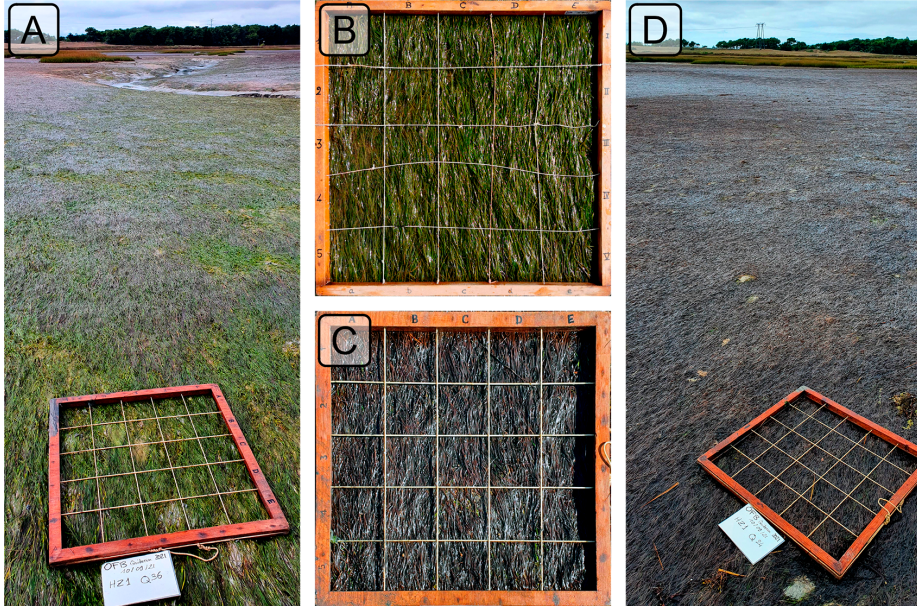


Figure 2: Illustrations of the two health conditions of seagrasses observed in the field. A: Global view of a green green meadow; B: Quadrat images of green seagrasses; C: Quadrat images of darkened seagrasses; D: Global view of an darkened meadow. All images were taken on September 10th, 2021, in Quiberon.

### 2.1.2. Temperature Data and identification of heatwaves

#### 2.1.2.1. Air temperature.

Since January 1, 2024, Meteo France weather data has been freely and openly accessible. Hourly air temperature data ( $^{\circ}\text{C}$ ) for the French Atlantic and Channel coasts was retrieved using a [custom script](#) as no API was available at the time of this study. Weather stations located within 10 kilometers of the coastline were considered, but only those with at least 30 years of data were included to ensure reliable climatological reconstruction. Of the 156 weather stations within 10 kilometers of the coast, only 36 had sufficient data for climatology reconstruction. The hourly data was then aggregated into daily mean temperatures for each station.

Heatwave detection was performed using the HeatwaveR package in R [24].

This package utilizes the methodology proposed by [13] to detect heatwave events. The climatology for the year was computed using the temperature time series. An event was considered a heatwave each time the temperature exceeded the 90th percentile of the climatology for three consecutive days. The severity of each event has been assessed using the methodology proposed by [25]. Following the methodology of [26], coldspell events corresponding to temperature below the percentile 10th of the climatology during 3 consecutive days have also been measured.

Concerning heatwaves event near Quiberon, this methodology has been applied solely on the nearest weather station of our study site (Lorient-Lann Bihoue, 47°45'46"N 3°26'11"W, more than 395000 observation since the 1st of February 1952).

#### *2.1.2.2. Water temperature.*

SST data from the Copernicus CMEMS platform were downloaded for the French coast near Quiberon (47°29'03" N, 3°07'09" W), covering 1982-2022 [27]. Only pixels within an area of 2700 km<sup>2</sup> around Quiberon, Brittany, France (47°29'03" N, 3°07'09" W) were extracted and analyzed. This area was large enough to minimize missing values caused by cloud cover, yet small enough to avoid being influenced by the stability of offshore SST. The multi-sensor Level 3S Sea Surface Temperature (SST) product we used is built from nighttime infrared satellite data, including sources like ESA SST CCI, C3S, and EUMETSAT. Data from AVHRR, ATSR, and SLSTR radiometers are used, but only those with a quality level above 4. An intercalibration method ensures consistency, and a daily reference SST field is constructed by combining the best data with median values from other sources. A large-scale bias correction is applied, and daily single-sensor composites are merged into a multi-sensor file (L3S), selecting the best sensor for each grid cell. A daily average was computed for the time series, and the HeatwaveR package [24] was used to compute SST climatology and detect SST events using the same method as air temperature event detection.

#### *2.1.3. Satellite Observation*

Two Sentinel-2 images covering the field trip site (Figure 1) were downloaded from the Copernicus platform [28]. The first image was taken before the heatwave event on September 1, 2021, and the second one after the event on September 6, 2021. Both images were acquired at Level-2 processing, in surface reflectance, and were orthorectified and atmospherically corrected to account for the effects of the atmosphere on reflectance values [29].

Reflectance value of each GCPs (Figure 1) have been extracted and compared before and after the heatwave event.

## 2.2. Laboratory experiment

### 2.2.1. Sampling and acclimation of seagrasses

Seagrass was sampled from a *Nanozostera noltei* (dwarf eelgrass, syn. *Zostera noltei*) meadow on Noirmoutier Island, France ( $46^{\circ}57'32.0''N$ ,  $2^{\circ}10'37.0''W$ ) at low tide in June 2024. A home-made inox sampling box was used to sample seagrass from an area of 30 cm by 15 cm and 5 cm deep, maintaining the sediment structure and avoiding damage to the rhizomes and the leafs of the seagrass (Figure 3 A). This sampling box allowed to limitate sampling variability between replicates. The entire system, including seagrass, sediment, meiofauna, and macrofauna, was placed in plastic trays together in a mesocosm setup, which allowed for the natural interactions between components to be maintained and reduced stress on the seagrass. To avoid hydric stress during transportation, seawater was added to each tray. Simultaneously, seawater was sampled from a nearby site and transported to the lab, where it was filtered using a 0.22  $\mu m$  nitrocellulose filter to remove all suspended particulate matter. This seawater was used in the acclimation tank and the intertidal chambers. The seagrasses were acclimated at high tide for one weeks with a water temperature of 17°C, matching the temperature at the time of sampling, and with light of 150 pmol.s<sup>-1</sup>.m<sup>-2</sup> of PAR photons [22]. A wave generator was used in the tank to circulate and reoxygenate the water.

### 2.2.2. Experimental design



Figure 3: Illustrations of the various steps of the experiment. A: Field sampling of seagrass using a homemade sampling box; B: Intertidal chambers used during the experiment; C: Seagrass sample inside a chamber during the experiment at high tide; D: Photo of the treatment sample at the start of the experiment; E: Photo of the treatment sample at the end of the experiment.

Two intertidal chambers from [ElectricBlue](#) were used to simulate tidal cycles and control water temperature during high tide and air temperature during low tide (Figure 3 B,C). One chamber served as the control, while the other was used for the experimental treatment.

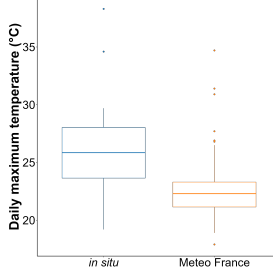


Figure 4: Comparison of daily maximum temperatures in August measured using an *in-situ* sensor (blue) and retrieved from Meteo France (orange). The solid line in the middle of the boxplot represents the median, the two ends of the box represent the 25th and 75th percentiles, and the whiskers represent values that are no more than 1.5 times the interquartile range.

To experimentally apply temperatures that closely mimic those experienced by seagrasses in the field, *in situ* temperature sensors were placed at the sampling site in Bourgneuf Bay during August 2024. The daily maximum temperatures recorded by the *in situ* sensors were compared to those measured by the nearest weather station operated by Meteo France (Figure 4). On average, *in situ* temperatures were  $3 \pm 3.2^\circ\text{C}$  higher than those recorded by Meteo France. Additionally, Meteo France temperatures were more stable compared to those from the *in situ* sensor. This stability is explained by the fact that Meteo France temperatures are measured in a sheltered, shaded location. This offset was used to adjust heatwave temperatures measured by Meteo France to reflect the conditions experienced by the seagrasses.

The control chamber was maintained at temperatures representative of the typical seasonal conditions: water temperatures between  $18^\circ\text{C}$  and  $19^\circ\text{C}$  and air temperatures between  $18^\circ\text{C}$  and  $23^\circ\text{C}$ , following circadian temperature variability (Figure 5 left). For the experimental treatment, the air temperature was set to mimic an atmospheric heatwave that occurred over the seagrass meadow of Quiberon, France ( $47^{\circ}35'40.0''\text{N}$ ,  $3^{\circ}07'30.0''\text{W}$ ) from September 2, 2021, to September 6, 2021. On the first day of the experiment, air temperatures in the experimental chamber were set to range from  $23^\circ\text{C}$  at night to  $35^\circ\text{C}$  during the day, with a daily increase of  $1^\circ\text{C}$ . The water temperature in the experimental chamber was similarly adjusted to reflect the heatwave conditions, starting from the normal seasonal range ( $18^\circ\text{C}$ ) and gradually increasing to simulate the rising temperatures experienced during the heatwave ( $+0.5^\circ\text{C}$  daily). This setup aimed to replicate the thermal stress experienced by the seagrass meadow during the actual heatwave event (Figure 5 right). The experiment stops only when no changes in the reflectance of the treatment are observed for 2 consecutive days.

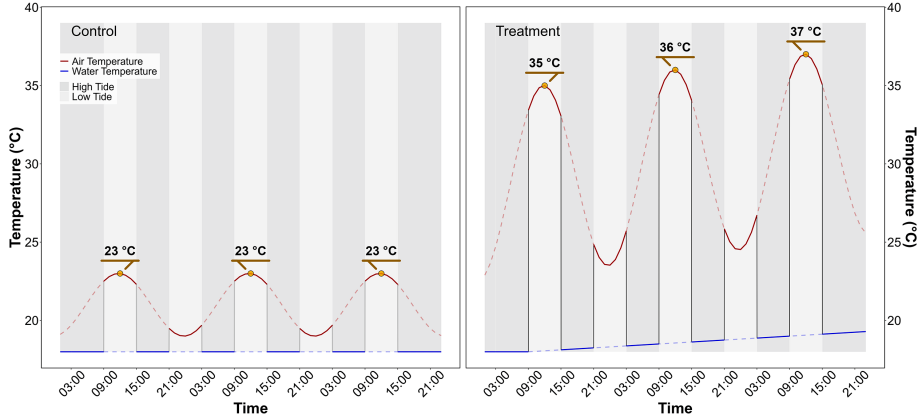


Figure 5: Temperature profiles of both the control (left) and the treatment (right) followed during the heatwave experiment. The red line indicates air temperature, whereas the blue line indicates water temperature. Due to the tidal cycle followed during the experiment, the seagrasses only experience temperatures represented by solid lines.

### 2.2.3. Bio-optical measurements over seagrass leaves

#### 2.2.3.1. Hyperspectral measurements.

Throughout the experiment, hyperspectral signatures of both the control and treatment seagrasses were taken using an ASD HandHeld 2 equipped with a fiber optic, allowing measurements to be taken directly inside the chamber without opening it. Automatic spectra acquisition has been done using the [RS3 software](#) developed by the instrument manufacturer. An average of five reflectance spectrum ( $R(\lambda)$ ), each with an integration time of 544 ms, was taken every minute. Every 10 minutes, the fiber optic was switched from one benthic chamber to the other, in order to measure reflectance in both treatment and control. Because light conditions were controlled inside of the chambers, reflectance calibration of the instrument was performed only each morning at the very first moment of low tide using a Spectralon white reference with 99% Lambertian reflectivity.

The second derivative of  $R$  was calculated to retrieve absorption features and compare their variability over time. Two radiometric indices were also monitored throughout the experiment :

- The Normalized Difference Vegetation Index (NDVI, [30]), as a proxy of the concentration of chlorophyll-a (Equation 1)

$$NDVI = \frac{R(840) - R(668)}{R(840) + R(668)} \quad (1)$$

where  $R(840)$  and  $R(668)$  are the reflectance at 840 nm and 668 nm respectively.

- The Seagrass Percent Covers, developed by [31], used to assess proportion of seagrass inside of a pixel (Equation 2):

$$SPC = 172.06 \times NDVI - 22.18 \quad (2)$$

- The Green Leaf Index (GLI, [32]), as a measurement of the greenness of seagrass leafs (Equation 3)

$$GLI = \frac{[R(550) - R(668)] + [R(550) - R(450)]}{(2 \times R(550)) + R(668) + R(450)} \quad (3)$$

where  $R(550)$  and  $R(450)$  are the reflectance in green at 550 nm and in the blue at 450 nm, respectively.

- The Mid-Infrared Water Absorption Index (MIWAI), proposed here and designed to measure water absorption at 970 nm (**REF**), estimates the difference between the reflectance at 970 nm and a linear interpolation of the reflectance values at 950 and 990 nm. This interpolation represents the expected reflectance value in the absence of water.

$$MIWAI = 0.5 \times [R(990) + R(950)] - R(970) \quad (4)$$

where  $R(990)$ ,  $R(970)$  and  $R(950)$  are the reflectance in the infrared at 990, 970 and 950 nm, respectively.

#### *2.2.3.2. Multispectral imagery measurement.*

Parallel to hyperspectral measurements, multispectral images were taken at the beginning and end of each diurnal low tide (09:00 am and 03:00 pm). A Micasense RedEdge-MX Dual multispectral camera, originally designed to be mounted on a drone, was modified for use without a drone. A 3D-printed mount was designed to attach the camera to the intertidal chamber and ensure that each picture was captured under the same conditions. At each time step (09:00 am and 03:00 pm), a first picture of the Spectralon was taken to allow for image correction in reflectance, followed by a second picture of the target. **DISCOV**, a Neural Network classification model previously developed to map intertidal vegetation using drone imagery, has been applied to each image taken inside the intertidal chambers. To understand the behavior of the model on seagrasses affected by heatwaves, classification images from before and after the heatwave have been compared.

### *2.2.3.3. Pigment concentration measurements.*

At the beginning and the end of each diurnal low tide (09:00 am and 03:00 pm) leaves samples have been took in both the test and the control. leaves sampled have been stored under -80°C waiting for analysis. Before pigment extraction, each sample was lyophilized and its dry weight was measured. Pigment composition and biomass were analyzed using high-performance liquid chromatography (HPLC). The HPLC system (Alliance HPLC 248 System, Waters) was equipped with a reverse-phase C-18 separating column (SunFire C-18 Column, 100Å, 3.5 µm, 2.1 mm x 50 mm, Waters), preceded by a precolumn (VanGuard 3.9 mm x 5 mm, Waters). The system also included a photodiode array detector (2998 PDA) and a fluorimeter (Ex: 425 nm, Em: 655 nm; RF-20A, SH

**Au secours Philippe !!!**

## **3. Results**

### *3.1. Heatwaves of Quiberon*

#### *3.1.1. Spectral inspection*

The Sentinel-2 images used in this study are dated from the 1st of September 2021 and the 6th of September 2021 (Figure 6 A and C, respectively). The Atmospheric Heat Wave (AHW) started on 4 September and lasted until 7 September, while the Marine Heat Wave (MHW) started on 3 September and ended on 8 September 2021 (Figure 6 B). The AHW has been classified as a strong event, and the MHW has been classified as moderate. Even though the Sentinel-2 of the 6th of September was captured only a few days after the start of the events, darkening of seagrass can already be observed in the true-color composition (Figure 6 C). Before the event, all GCPs appeared green un the images, with similar reflectance spectra, regardless of the class attributed to the GCPs on the field (Figure 6 A and D left). Their reflectance spectra showed a peak at 560 nm (in the green part of the spectra), low values at 665 nm, corresponding to the strong absorption by chlorophyll-a and a high infrared plateau ( $> 705$  nm). However, GCPs classified as dark seagrass during the fieldtrip, showed significant differences in reflectance spectral shape compared to GCPs classified as green seagrass on the 10th of September, with corresponding differences in the true color composition (Figure 6 C and D right). In fact these dark seagrass GCPs were affected by extreme events, which altered their color and impacted the satellite reflectance (Figure 6 C). The reflectance spectra over dark seagrass were characterized by the loss of the reflectance peak at 560 nm and a decrease in the infared plateau, which was observed as a steady increasing slope up to 940 nm.

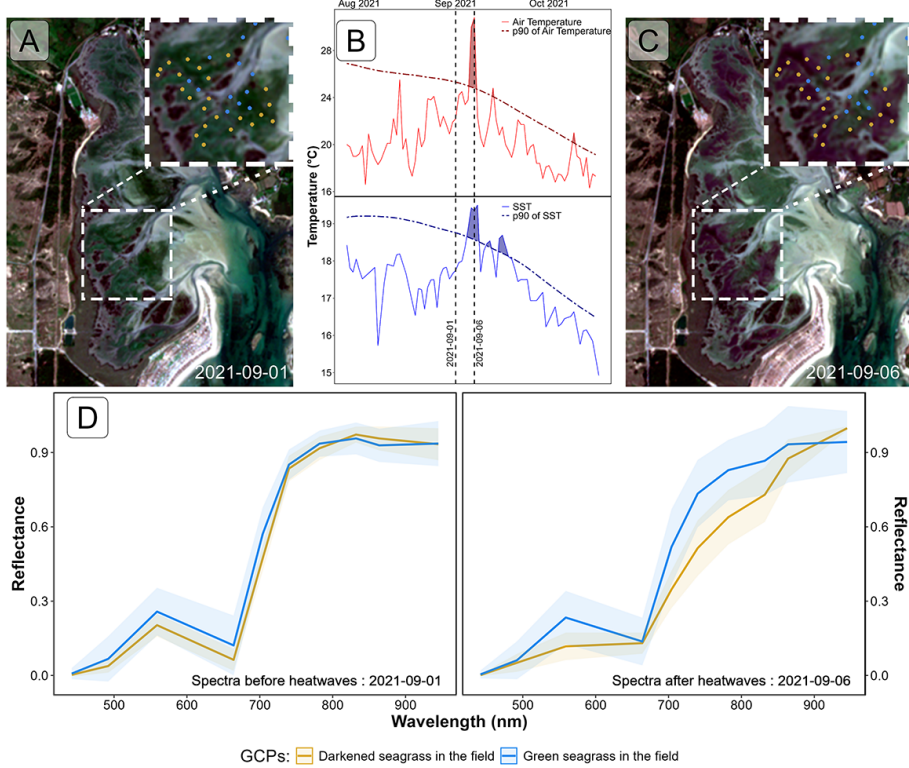


Figure 6: Spectral Comparison of Sentinel-2 Reflectance (D) over Ground Control Points (GCPs) Before (A) and During (B) Heatwave Events (C); A: RGB color composition of the Sentinel-2 image on the 1st of September 2021. The points correspond to GCPs collected on September 10, 2021 Figure 1; B: Detection of heatwave events based on both Air Temperature and Sea Surface Temperature (SST). The solid line represents the daily average temperature, while the dashed line indicates the 90th percentile of the climatology. Colored polygons identify heatwaves (marine in blue and atmospherical in red). The two vertical dashed lines represent the acquisition dates of the two Sentinel-2 images used in this analysis ; C : RGB color composition of the Sentinel-2 image on the 6th of September 2021. The points correspond to GCPs collected on September 10, 2021 Figure 1 ; D : Average spectral signatures of GCPs where dark and green seagrasses (blue and gold lines, respectively) were identified during the field survey. The left plot shows the reflectance of these GCPs before the heatwave impact, while the right plot shows the spectral signature during the heatwaves. The ribbons around the lines represent the standard deviation.

### 3.1.2. Radiometric indices comparison

Using Sentinel-2 reflectance values extracted from GCPs before and during the events, radiometric indices were calculated and compared. Column A of Figure 7, which represents indices from GCPs classified as green seagrass during the field trip on September 10th (i.e., seagrass not affected by the heatwave events), shows no notable differences before or during the event, regardless of the index. However, Column B of Figure 7 shows significant differences in the indices of GCPs classified as darkened seagrass during the same field trip (i.e.,

seagrass affected by the heatwave events).

The NDVI dropped from a median of 0.61 to 0.40, while also becoming less variable (standard deviation decreasing from 0.09 to 0.06) (Figure 7 B1). Although the seagrass density remained consistent before and during the event, the drop in NDVI affected the retrieved Seagrass Percent Cover (SPC) values (Figure 7 B2). The SPC decreased from a median of 83% before the event to 48% during the event. A similar trend is observed with the GLI, which dropped from a median of 0.15 before the event to 0.02 after the event (Figure 7 B3).

Interestingly, the density of seagrass that remained green after the event (median SPC = 65%; Figure 7 A2) was initially lower than the density of seagrass that darkened (median SPC = 85%; Figure 7 B2).

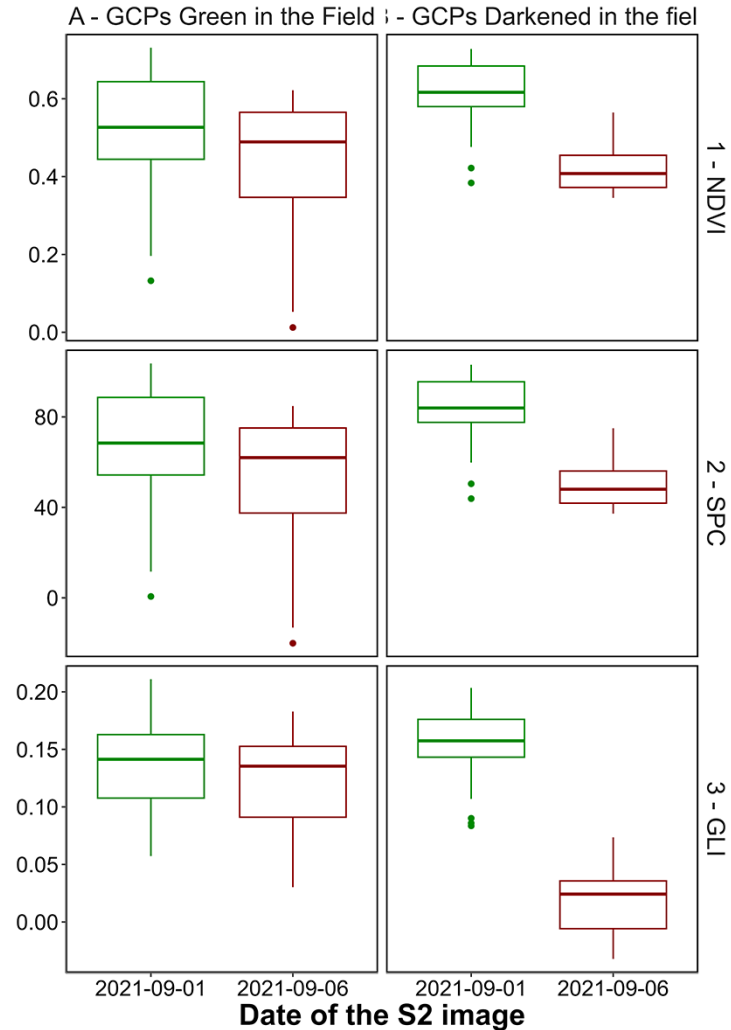


Figure 7: Comparaison of Sentinel-2 based radiometric indices at two different dates, before (2021-09-01, green) and after (2021-09-06, red) the heatwaves events of Quiberons, for the two category of GCPs seen in the field : Green seagrasses (Column A) and Darkened Seagrasses (Column B). The Normalised Difference Vegetation Index (1-NDVI) has been computed using the Equation 1, the Seagrass Percent Cover (2-SPC) with the Equation 2 and the Green Leaf Index (3-GLI) using Equation 3,

## Bibliography

- [1] R. K. Unsworth, L. C. Cullen-Unsworth, B. L. Jones, R. J. Lilley, The planetary role of seagrass conservation, *Science* 377 (6606) (2022) 609–613.
- [2] A. I. Sousa, J. F. da Silva, A. Azevedo, A. I. Lillebø, Blue carbon stock

in *Zostera noltei* meadows at ria de aveiro coastal lagoon (portugal) over a decade, *Scientific reports* 9 (1) (2019) 14387.

- [3] M. L. Zoffoli, P. Gernez, L. Godet, S. Peters, S. Oiry, L. Barillé, Decadal increase in the ecological status of a north-atlantic intertidal seagrass meadow observed with multi-mission satellite time-series, *Ecological Indicators* 130 (2021) 108033.
- [4] E. Jankowska, L. N. Michel, G. Lepoint, M. Włodarska-Kowalcuk, Stabilizing effects of seagrass meadows on coastal water benthic food webs, *Journal of Experimental Marine Biology and Ecology* 510 (2019) 54–63.
- [5] M. L. Zoffoli, P. Gernez, S. Oiry, L. Godet, S. Dalloyau, B. F. R. Davies, L. Barillé, Remote sensing in seagrass ecology: coupled dynamics between migratory herbivorous birds and intertidal meadows observed by satellite during four decades, *Remote Sensing in Ecology and Conservation* 9 (3) (2023) 420–433.
- [6] R. C. Gardner, C. Finlayson, Global wetland outlook: state of the world's wetlands and their services to people, in: Ramsar convention secretariat, 2018, pp. 2020–5.
- [7] A. L. Scott, P. H. York, C. Duncan, P. I. Macreadie, R. M. Connolly, M. T. Ellis, J. C. Jarvis, K. I. Jinks, H. Marsh, M. A. Rasheed, The role of herbivory in structuring tropical seagrass ecosystem service delivery, *Frontiers in Plant Science* 9 (2018) 127.
- [8] C. Ramesh, R. Mohanraju, Seagrass ecosystems of andaman and nicobar islands: Status and future perspective., *Environmental & Earth Sciences Research Journal* 7 (4) (2020).
- [9] M. Waycott, C. M. Duarte, T. J. Carruthers, R. J. Orth, W. C. Dennison, S. Olyarnik, A. Calladine, J. W. Fourqurean, K. L. Heck Jr, A. R. Hughes, et al., Accelerating loss of seagrasses across the globe threatens coastal ecosystems, *Proceedings of the national academy of sciences* 106 (30) (2009) 12377–12381.
- [10] E. Thomsen, L. S. Herbeck, I. G. Viana, T. C. Jennerjahn, Meadow trophic status regulates the nitrogen filter function of tropical seagrasses in seasonally eutrophic coastal waters, *Limnology and Oceanography* 68 (8) (2023) 1906–1919.
- [11] K. Sevgi, S. Leblebici, Bitkilerde ağır metal stresine verilen fizyolojik ve moleküler yanıtlar, *Journal of Anatolian Environmental and Animal Sciences* 7 (4) (2022) 528–536.
- [12] T. S. Simpson, T. Wernberg, J. I. McDonald, Distribution and localised effects of the invasive ascidian *didemnum perlucidum* (monniot 1983) in an urban estuary, *PLoS One* 11 (5) (2016) e0154201.

- [13] A. J. Hobday, L. V. Alexander, S. E. Perkins, D. A. Smale, S. C. Straub, E. C. Oliver, J. A. Benthuysen, M. T. Burrows, M. G. Donat, M. Feng, et al., A hierarchical approach to defining marine heatwaves, *Progress in oceanography* 141 (2016) 227–238.
- [14] S. E. Perkins, L. V. Alexander, On the measurement of heat waves, *Journal of climate* 26 (13) (2013) 4500–4517.
- [15] Y. Sawall, M. Ito, C. Pansch, Chronically elevated sea surface temperatures revealed high susceptibility of the eelgrass *zostera marina* to winter and spring warming, *Limnology and Oceanography* 66 (12) (2021) 4112–4124.
- [16] A. Deguette, I. Barrote, J. Silva, Physiological and morphological effects of a marine heatwave on the seagrass *cymodocea nodosa*, *Scientific Reports* 12 (1) (2022) 7950.
- [17] G. Winters, P. Nelle, B. Fricke, G. Rauch, T. B. Reusch, Effects of a simulated heat wave on photophysiology and gene expression of high-and low-latitude populations of *zostera marina*, *Marine Ecology Progress Series* 435 (2011) 83–95.
- [18] L. Guerrero-Meseguer, A. Marín, C. Sanz-Lázaro, Heat wave intensity can vary the cumulative effects of multiple environmental stressors on *posidonia oceanica* seedlings, *Marine Environmental Research* 159 (2020) 105001.
- [19] A. R. Huete, Vegetation indices, remote sensing and forest monitoring, *Geography Compass* 6 (9) (2012) 513–532.
- [20] S. Kloos, Y. Yuan, M. Castelli, A. Menzel, Agricultural drought detection with modis based vegetation health indices in southeast germany, *Remote Sensing* 13 (19) (2021) 3907.
- [21] I. Cârlan, B.-A. Mihai, C. Nistor, A. Große-Stoltenberg, Identifying urban vegetation stress factors based on open access remote sensing imagery and field observations, *Ecological Informatics* 55 (2020) 101032.
- [22] M. Akbar, P. Arisanto, B. Sukirno, P. Merdeka, M. Priadhi, S. Zallesa, Mangrove vegetation health index analysis by implementing ndvi (normalized difference vegetation index) classification method on sentinel-2 image data case study: Segara anakan, kabupaten cilacap, in: IOP Conference Series: Earth and Environmental Science, Vol. 584, IOP Publishing, 2020, p. 012069.
- [23] E. Papathanasopoulou, S. Simis, K. Alikas, A. Ansper, J. Anttila, A. Barillé, L. Barillé, V. Brando, M. Bresciani, M. Bučas, et al., Satellite-assisted monitoring of water quality to support the implementation of the water framework directive, EOMORES white paper (2019).

- [24] R. W. Schlegel, A. J. Smit, heatwaveR: A central algorithm for the detection of heatwaves and cold-spells, *Journal of Open Source Software* 3 (27) (2018) 821. [doi:10.21105/joss.00821](https://doi.org/10.21105/joss.00821).
- [25] A. J. Hobday, E. C. Oliver, A. S. Gupta, J. A. Benthuysen, M. T. Burrows, M. G. Donat, N. J. Holbrook, P. J. Moore, M. S. Thomsen, T. Wernberg, et al., Categorizing and naming marine heatwaves, *Oceanography* 31 (2) (2018) 162–173.
- [26] R. W. Schlegel, E. C. Oliver, T. Wernberg, A. J. Smit, Nearshore and offshore co-occurrence of marine heatwaves and cold-spells, *Progress in Oceanography* 151 (2017) 189–205.
- [27] CMEMS, European north west shelf/iberia biscay irish seas – high resolution odyssea sea surface temperature multi-sensor l3 observations reprocessed, e.u. copernicus marine service information (cmems). marine data store (mds). (accessed on 17-10-2024) (2024). [doi:10.48670/moi-00311](https://doi.org/10.48670/moi-00311).
- [28] European Space Agency, Copernicus open access hub, <https://scihub.copernicus.eu>, accessed: 2024-10-20 (2024).
- [29] European Space Agency, Sen2cor: Sentinel-2 atmospheric correction processor, <https://step.esa.int/main/third-party-plugins-2/sen2cor/>, accessed: 2024-10-20 (2024).
- [30] J. W. Rouse, R. H. Haas, J. A. Schell, D. W. Deering, et al., Monitoring vegetation systems in the great plains with erts, *NASA Spec. Publ* 351 (1) (1974) 309.
- [31] M. L. Zoffoli, P. Gernez, P. Rosa, A. Le Bris, V. E. Brando, A.-L. Barillé, N. Harin, S. Peters, K. Poser, L. Spaias, et al., Sentinel-2 remote sensing of *zostera noltei*-dominated intertidal seagrass meadows, *Remote Sensing of Environment* 251 (2020) 112020.
- [32] M. Louhaichi, M. M. Borman, D. E. Johnson, Spatially located platform and aerial photography for documentation of grazing impacts on wheat, *Geocarto International* 16 (1) (2001) 65–70.